International Journal of Scientific Research in Engineering and Management (IJSREM)
Volume: 09 Issue: 03 | March - 2025 SJIF Rating: 8.586 ISSN: 2582-3930

Effect of G-Phase Precipitation on Creep-Damaged SS 347H Platen Superheater Boiler Tube Failure

Dr R K Kumar[1], D Laxman Rao[2]

Materials Technology Division,
Central Power Research Institute, Bangalore

Abstract

The failure of a platen superheater tube of SA213-TP347H grade austenitic stainless steel was investigated through chemical, metallurgical, mechanical, and microstructural analysis and scanning electron microscopy. A marginal reduction in hardness of the serviced tube with depletion of chromium in the matrix compared to the virgin tube material was observed. While the yield and tensile strengths remained within limits, the elongation property was decreased significantly, indicating the occurrence of localized embrittlement. The effect of the complex silicide phase in the matrix in conjunction with $Cr_{23}C_6$ precipitates along the grain boundaries on the embrittlement of tube material has been studied. These findings emphasize the role of microstructural stability in premature tube failures under high-temperature environments.

***Keywords*:** Silicide phase, silicon enrichment, austenitic stainless steel, $Cr_{23}C_6$, embrittlement, Creep

1. Introduction

Boilers in thermal power plants consist of several critical components, including economizers, water walls, superheaters, and reheaters. Boiler tube failure is a common cause of unscheduled outages in a thermal power plant component**.** Different damage mechanisms like creep, fatigue, erosion, and corrosion are responsible for the boiler failure of varying pressure parts tubes.

The generation loss due to forced outages due to the failure of boiler tubes in Indian thermal plants during 2017-18 increased to 19.09% compared to 12.23% during 2012-13 [1]. The most common failures in boilers are caused by long-term overheating in superheaters and reheaters, operating at high steam temperature conditions. Since the superheater tubes are exposed to steam temperature conditions, they are highly susceptible to failure in service. The SS347 stainless steel grade is commonly used for the lower regions of pendant coils where the flue gas temperature is maximum. Shuro et al. (2012) reported that G-phase precipitation, an Mn–Ni–Si-rich silicide phase, occurs in high-pressure torsion-deformed SUS304 stainless steel, resulting in significant embrittlement [2]. The G-phase, a silicide-rich precipitate formed during thermal ageing in duplex stainless steel, significantly influences the material's microstructure and mechanical properties by exhibiting a morphology governed by the misfit degree between the G-phase and the matrix [3]. The study by Guo et al. highlighted that the formation of G-phase (Ni-Nb silicide) in 20Cr32Ni1Nb stainless steel significantly contributes to the degradation of mechanical properties, and phase transformation of NbC into G-phase during service exposure [4]. The presence of G-phase (silicide) precipitates in localized chromium-enriched regions of Type 316H austenitic stainless steel significantly influences the material's creep behaviour and contributes to the development of localized creep cracks during service [5]. Swaminathan et al. (2011) concluded that the failure of AISI 347 stainless steel tubes due to intergranular stress corrosion cracking (IGSCC) was predominantly a result of sensitization, which was likely induced by localized overheating [6]. The sensitization of 304H stainless steel superheater tubes significantly contributed to intergranular stress corrosion cracking (IGSCC), demonstrating the critical influence of microstructural changes on failure mechanisms in high-temperature applications[7].

Fig. 1 Failed Platen Superheater Tube

Understanding the root cause of such failures is crucial for improving operational reliability and extending the service life of critical components. In this study, a failed platen superheater tube made of SA213 TP347H stainless steel was analyzed to determine the underlying causes of its premature failure. One failed V-type bend tube, with a length of 400 mm, was used for the analysis (Fig. 1). The material specifications, design details, and operating parameters of the failed platen superheater tube are provided in Table 1. The location of the tube failure inside the boiler is shown in Fig. 2.

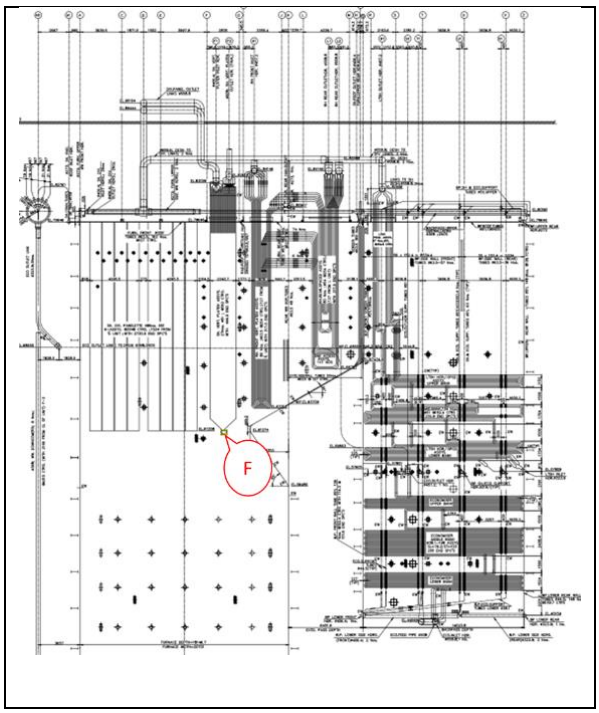

Fig 2. View of the Failed Tube location inside the Boiler tube panel

Table 1: Details of the Plant and failed PSH tube

Capacity	600 MW
No. of Hours of service	60032 hrs.
Location of Tube	Coil No-12, Tube no-06.
Material of Tube	SA213-TP347H
Working pressure	Steam pressure-176 bar ; Temperature-540 ^{0}C
Outer diameter & Design thickness	51 mm x 7.5 mm
Flue gas temperature in the vicinity	1040 ^{0}C

A systematic failure investigation was conducted, encompassing visual examination, dimensional measurements, hardness evaluation, mechanical property testing, microstructural analysis, and scanning electron microscopy (SEM) with energy-dispersive X-ray spectroscopy (EDS).

2. Experimental Techniques and Results

2.1 Visual Examination

The failed tube exhibited a significant crack opening on the inner diameter (ID) side of the bend, along with multiple longitudinal cracks. The failure occurred at the bottom end of the "V" section of the superheater (SH) coil, with a blistered opening measuring 14 cm in length. The failed opening had shown multiple internal cracks close to the failure lip end region with a 25% reduction in wall thickness, as shown in Fig. 3. In addition, multiple longitudinal cracks adjacent to the failed opening, indicated that the tube had been subjected to excessive temperature and stress conditions during service (Fig. 4). The failed opening coincided with the observed longitudinal crack. The length of the crack opening boundary was measured to be 30 cm (Figure 4b).

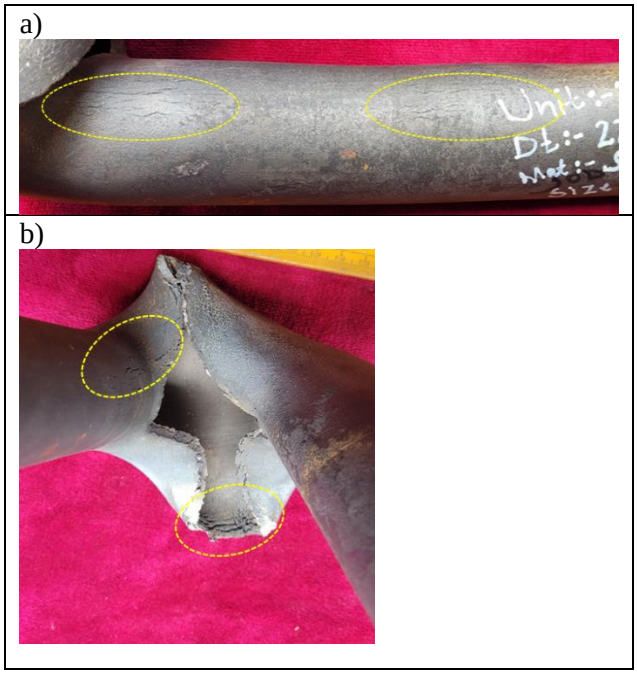

Fig. 3 Longitudinal cracks near the failure opening

2.2 Dimensional Measurement

To assess the possible swelling due to localized overheating, the tube thickness was measured along its length at intervals of 25 mm. The thickness of the tube in the failed opening has been observed to be 5.3 to 5.5 mm against the design thickness value of 7.0 mm. No reduction in wall thickness was observed in regions away from the failure. However, longitudinal multiple surface cracks were observed along the vertical length of the failed tube.

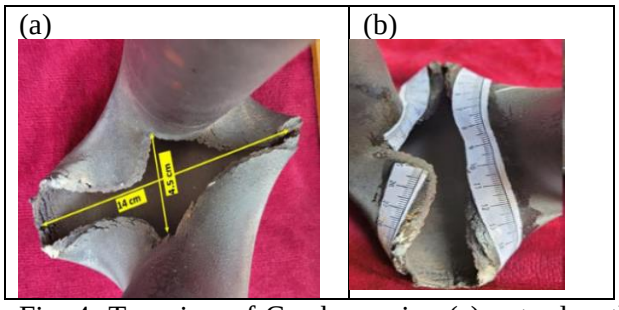

Fig. 4 Top view of Crack opening (a) outer length of the blister opening region (b)

2.3 Chemical Analysis

The chemical composition of the failed platen superheater tube was analyzed using an Optical Emission Spectrometer (OES). The analysis was conducted on both the failed and virgin tubes and the averaged results are summarized in Table 2.

Table -2: Chemical Composition Analysis

Composition, by weight %			
Elements	Failed Tube	New Tube	(Ref. Values - TP347H as per ASTM std.)
C	0.053	0.059	0.04-0.10
Mn	1.17	1.31	2 max.
Si	0.409	0.429	1 max.
P	0.02	0.019	0.045 max.
S	0.012	0.006	0.03 max.
Cr	16.83	17.17	17-19
Ni	11.93	11.37	9-13
Nb	0.59	0.68	8 x C – 1.2 max.

The elemental composition of both the failed and virgin tubes met the requirements as per ASTM A213 standard for TP347H grade steel[8].

2.4 Hardness Measurement

Hardness measurements were conducted using a rebound hardness tester in the Brinell Hardness (BHN) scale to assess temperature-induced physical changes in the tube material. The average hardness of the failed tube was observed to be in the range of 125–160 BHN**,** whereas for the new tube, the hardness value was observed in the range of 160-185 BHN. The reduced hardness value of the region away from the failure opening was observed, suggesting possible softening of the tube metal due to prolonged exposure at elevated temperature conditions.

2.5 Mechanical Properties Evaluation

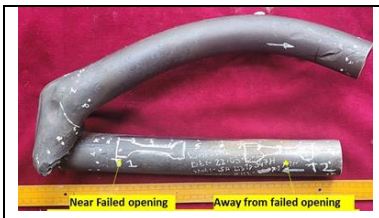

Fig . 5 Sample Location for Tensile Testing

Table -3: Summary of Mechanical Properties of Failed and Virgin Platen Superheater Tubes

Tube Description	Yield Strength (MPa)	Ultimate Strength (MPa)	Elongation (%)
Near Failed Opening (T1)	286	567	31.4
Away from Failure (T2)	314	599	32.3
Virgin Tube	257	571	43.3
Ref. Values (TP347H)	**> 205**	**> 485**	**> 35**

The yield strength and tensile strength of the failed tube were found to be within the acceptable range specified for the material. However, a significant reduction in elongation up to 26-28% compared to the virgin tube was observed in the failed tube samples,

2.6 Microstructural Examination

The metallurgical condition of the failed platen superheater tube was assessed through microstructural analysis at different locations. Small samples were extracted from various regions of the failed tube and prepared for optical microscopy. The specimens were polished and etched using aqua regia solution to reveal the grain boundaries, precipitates, carbide phases, and twin boundaries etc. The microstructural examination revealed the presence of austenitic grains with distinct twin boundaries and cracking from the ID side of the tube. The microstructures observed are shown in Fig. 7 and 8. The micrographs show clear evidence of intergranular cracking along the grain boundaries. Multiple cracks propagate along the grain boundaries indicating that the failure appears to be attributed to

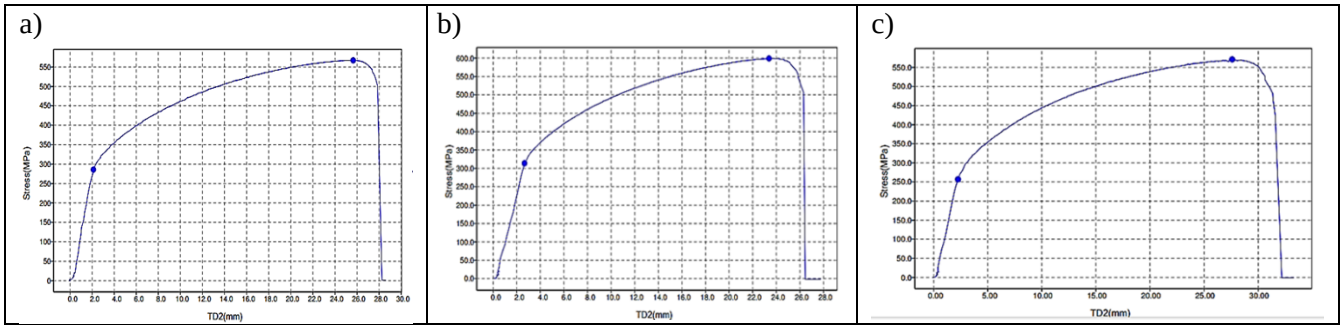

Fig 6. Stress-Displacement Graph of tensile tested samples ; Near failed Opening (a) away from failed opening (b) virgin tube (c) ; TD2 – Displacement

The mechanical properties of both the failed and virgin tubes were performed. Tensile samples were taken 150 mm away from the failure opening in the straight-length region (Fig. 5) and the tests were conducted as per ASTM E-8 /E8M-22 standards including yield strength, ultimate tensile strength, and elongation properties. The results were compared with that of the virgin tube property. The Load Displacement graphs of the tensile samples are shown in Fig 6. The results of the mechanical testing are given in Table 3.

creep-induced cracking mechanism.

2.7 SEM and EDX Analysis of the Failed Tube

The etched sample from the failed tube was analyzed using scanning electron microscopy (SEM) coupled with Energy Dispersive X-ray spectroscopy (EDS) for microstructural degradation and the presence of secondary precipitates.

The SEM analysis revealed fine precipitates distributed within the austenitic grains and larger secondary precipitates along the grain boundaries. The precipitation of fine NbC fine precipitates which are commonly found in stabilized stainless steels. The coarser precipitates of size 20 to 60 microns were also observed in the matrix region. The EDS analysis of the precipitate indicated a higher content of silicon and niobium with a reduced amount of chromium and nickel. The presence of these secondary phases suggests potential microstructural instability due to prolonged high-temperature exposure. This could contribute to localized embrittlement and increased susceptibility to high-temperature degradation. The SEM images illustrating these precipitates are shown in Fig 9. The EDS analysis of the precipitate rich in silicon is shown in Fig 10. The EDS spectrum obtained from the precipitate region rich in silicon is shown in Fig. 11. The precipitate regions exhibiting in-depth de-bonding were analyzed along the length direction to identify specific phases. Chromium and silicon content variation along a line scan was observed, as shown in Figures 12 and 13.

2.8 Analysis of tube ID Side Deposit

The ID Side deposit of the tube was analyzed for its concentration of different elements by the Energy Dispersive X-ray spectroscopy (EDS) method. The spectrum indicating different elements identified along with the results of Elemental quantification are given in Table 4. The ID Side oxide scale shows predominantly Silicon, Chromium, nickel, and sodium, apart from Iron and oxygen.

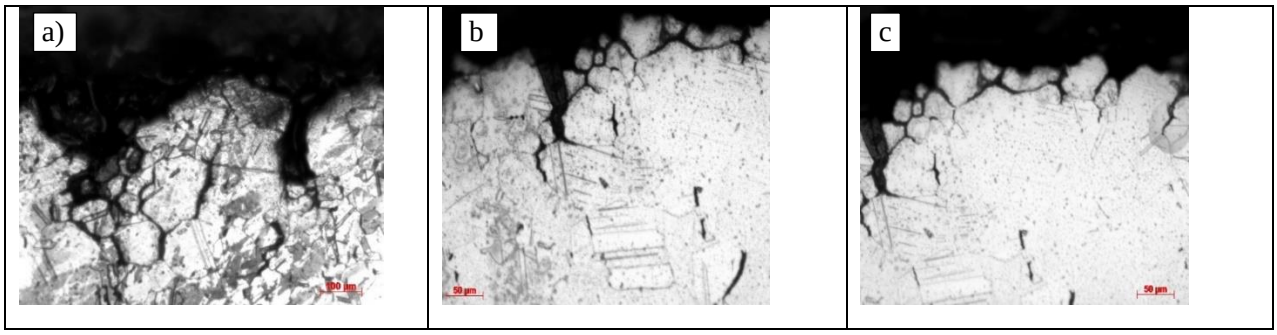

Fig 7. Microstructure of the failed tube near the failure opening showing multiple cracks joined along grain boundaries (a) (b) (c)

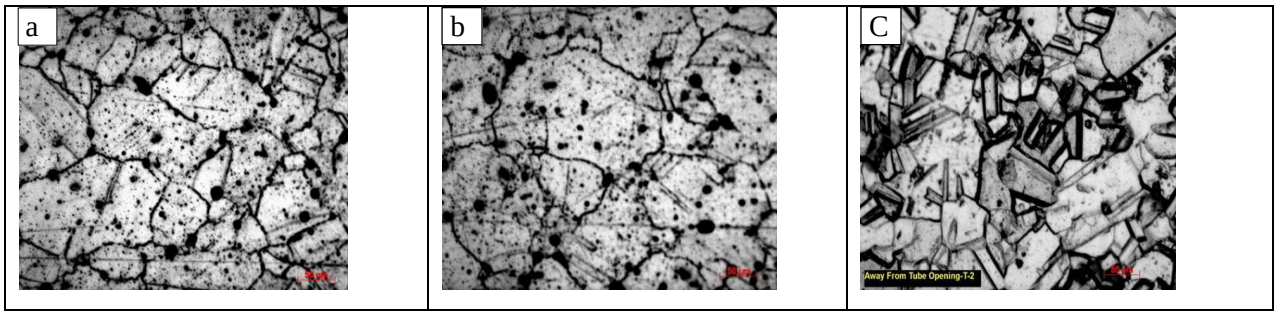

Fig 8. Microstructure of the failed tube near failed opening showing sensitized structure (a) (b) and virgin tube structure with twin (c)

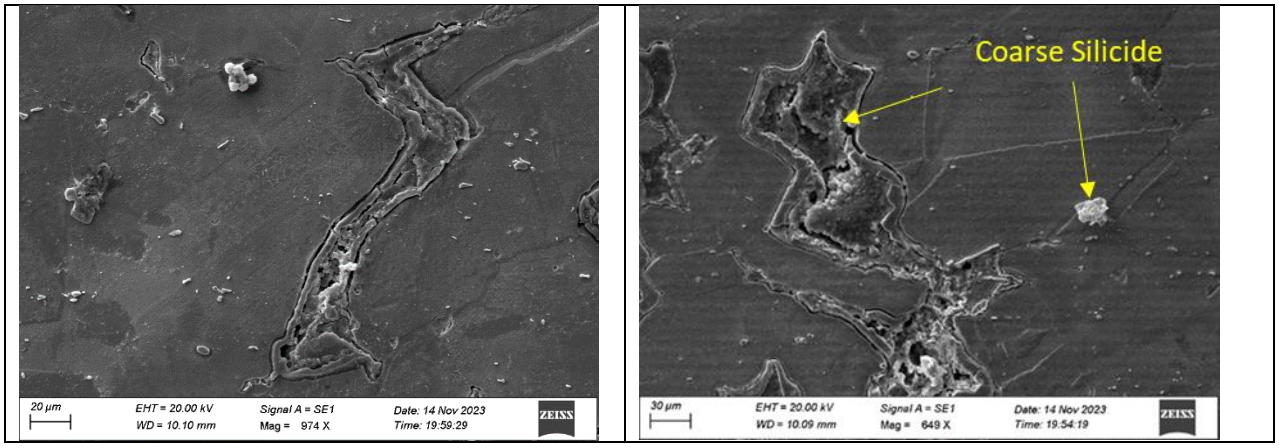

Fig. 9 Secondary Electron Micrographs of the sample near the failure opening showing thick precipitates with multiple cracks

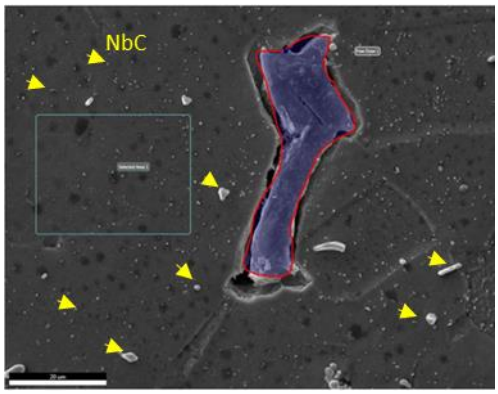

Matrix Region

Element	Weight %
Oxygen	1.52
Silicon	0.36
Niobium	4.74
Chromium	16.50
Manganese	1.62
Nickel	9.45
Iron	Balance

Precipitate Region

Element	Weight %
Oxygen	19.1
Silicon	17.42
Niobium	18.45
Chromium	8.45
Manganese	0.84
Nickel	3.71
Aluminium	1.42
Chlorine	3.62
Iron	Balance

Fig.10 EDS analysis of precipitate and matrix region

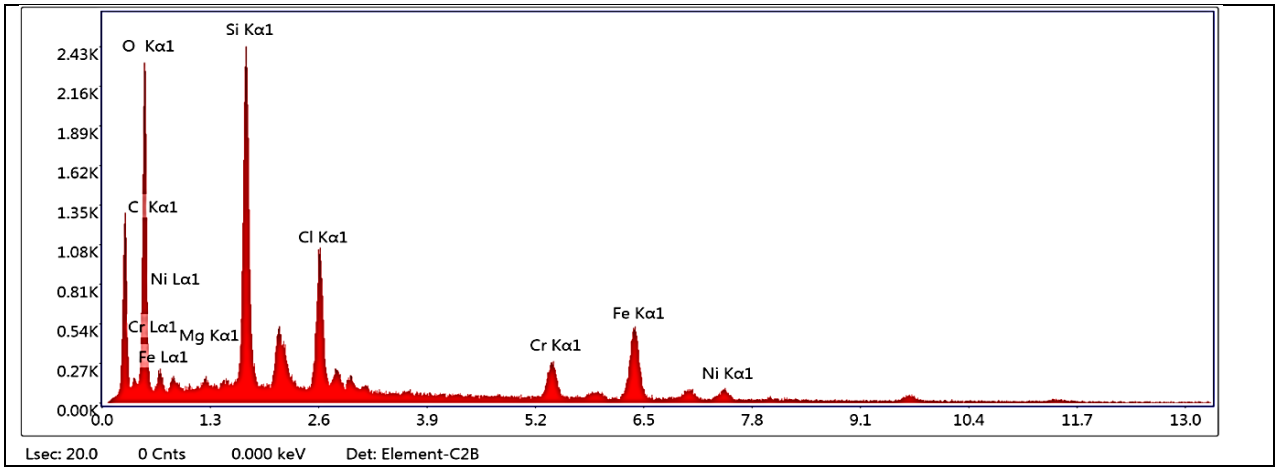

Fig.11 EDS Spectrum confirming the presence of high amount of silicon in precipitate

a)

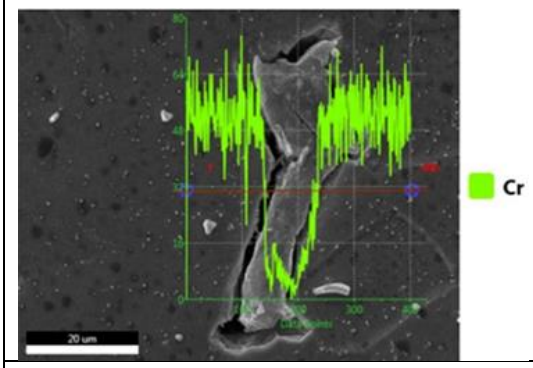

b)

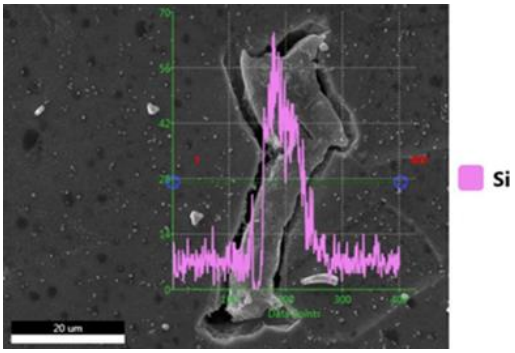

Fig.12 Line scan along the precipitate showing depletion of the Chromium (a) Silicon enrichment of the precipitate (b)

Table 4 EDS analysis results of ID side Deposit

Oxide Present	**Average ID Side Oxide Concentration (% wt.)**
Na_2O	1.46
MgO	0.57
Al_2O_3	1.77
SiO_2	6.69
K_2O	0.41
CaO	1.19
Cr_2O_3	20.57
Fe_2O_3	59.40
NiO	7.96

3.0 Result and Discussion

The chemical composition analysis of the failed tube conforms to SA213 TP347H steel. Thickness measurements near the failed opening show a marginal reduction in wall thickness up to 2.0 mm compared to the design thickness. The region away from the failure opening indicated a considerable reduction in hardness (125 to 138 BHN) against the virgin tube hardness values of 160 and 185 BHN**.**

The yield strength and tensile strength of the failed tube were within the ASTM-specified limits. However, the elongation values of the failed tube samples showed a 26 to 28% reduction in elongation compared to the virgin tube, indicative of localized embrittlement. The optical micrograph of the virgin tube indicated the prevalence of annealing twin structures within the austenitic grains. However, the microstructure near the failure region has indicated the grain growth with voids along the grain boundaries. The SEM micrographs indicated the presence of large-sized silicide precipitates (G-phase) of size up to 60 microns**,** at isolated locations. The formation of silicide precipitate is due to the interaction of silicon with NbC and chromium during long-term exposure to elevated temperature. The observed macro cracks along the longitudinal direction are indicative of the creep-induced damage in specific regions of the tube material.

Debonding between the precipitates and the matrix was evident, with cracks initiating at the precipitate-matrix interface. EDS analysis confirmed high silicon content (5–18%) in the precipitates, in contrast to a significantly lower silicon concentration (0.3–0.4%) inside the grains. Furthermore, EDS line mapping identified chromium depletion (<9%) near the precipitate-matrix interface and high silicon enrichment in the precipitates. Under high-temperature conditions of 600 to 800 °C, the diffusion rate of silicon is more than that of carbon. This results in faster coarsening and larger precipitate sizes for silicides. The coarse precipitates observed along the grain boundaries were identified as G-phase (complex silicides), which typically form after prolonged exposure to high temperatures**.**

Microstructural examination revealed G-phase silicides, with SEM-EDS confirming silicon-rich precipitates and chromium depletion near grain boundaries (Fig. 12).

EDS analysis of the inner diameter (ID) scale showed the presence of Fe_2O_3, Cr_2O_3, NiO, and SiO**,** indicating oxidation and scaling effects. The formation of the G

phase leads to the depletion of localized chromium and nickel and decreases ductility and corrosion resistance, which was evident in the failed tube.

The failure mechanism identified in the present study is given below.

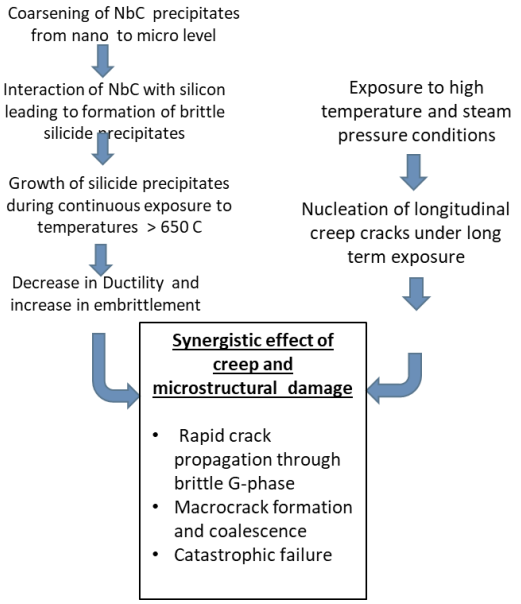

4.0 Conclusion

The failure of the platen superheater tube was attributed to the synergistic effect of high-temperature-induced precipitation of chromium-rich phases and silicide formation**,** which led to material embrittlement. The combination of localized deformation due to creep damage near the failed opening and reduced ductility due to G-phase precipitation ultimately resulted in tube failure.

ACKNOWLEDGEMENT

The authors sincerely acknowledge the support provided by the Central Power Research Institute (CPRI) for facilitating this investigation.

REFERENCES

[1] N. D. Central Electricity Authority, “Review of performance of Thermal Power Station, 2017-18,” 2020.

[2] I. Shuro, H. H. Kuo, T. Sasaki, K. Hono, Y. Todaka, and M. Umemoto, “G-phase precipitation in austenitic stainless steel deformed by high pressure torsion,” *Mater. Sci. Eng. A*, vol. 552, pp. 194–198, 2012, doi: 10.1016/j.msea.2012.05.030.

[3] Y. Chen, X. Dai, X. Chen, and B. Yang, “The characterization of G-phase in Fe20Cr9Ni cast duplex stainless steel,” *Mater. Charact.*, vol. 149, no. October 2018, pp. 74–81, 2019, doi: 10.1016/j.matchar.2019.01.012.

[4] X. F. Guo *et al.*, “Formation of G-phase in 20Cr32Ni1Nb stainless steel and its effect on mechanical properties,” *Acta Metall. Sin. (English Lett.*, vol. 30, no. 9, pp. 829–839, 2017, doi: 10.1007/s40195-017-0589-0.

[5] A. D. Warren, I. J. Griffiths, and P. E. J. Flewitt, “Precipitation within localised chromium-enriched regions in a Type 316H austenitic stainless steel,” *J. Mater. Sci.*, vol. 53, no. 8, pp. 6183–6197, 2018, doi: 10.1007/s10853-017-1748-4.

[6] J. Swaminathan, R. Singh, M. K. Gunjan, and B. Mahato, “Sensitization induced stress corrosion failure of AISI 347 stainless steel fractionator furnace tubes,” *Eng. Fail. Anal.*, vol. 18, no. 8, pp. 2211–2221, 2011, doi: 10.1016/j.engfailanal.2011.07.015.

[7] A. S. Abou-elazm, I. El Mahallawi, R. Abdel-karim, and R. Rashad, “Failure investigation of secondary super-heater tubes in a power boiler,” *Eng. Fail. Anal.*, vol. 16, no. 1, pp. 433–448, Jan. 2009, doi: 10.1016/j.engfailanal.2008.06.024.

[8] ASTM, “A213-11a Standard Specification for Seamless Ferritic and Austenitic Alloy-Steel Boiler , Superheater , and Heat-Exchanger Tubes 1 A262 Practices for Detecting Susceptibility to Intergranular,” vol. i, 2014, doi: 10.1520/A0213.